Biosensors and Bioelectronics 32 (2012) 127–132

Contents lists available at SciVerse ScienceDirect

Biosensors and Bioelectronics

journal homepage: www.elsevier.com/locate/bios

Gold-based optical biosensor for single-mismatched DNA detection using salt-induced hybridization

Zongrui Zhan [a], Xingyi Ma [b], Cuong Cao [c], Sang Jun Sim [b,*]

[a] Department of Chemical Engineering, Sungkyunkwan University, Suwon 440-746, South Korea
[b] Department of Chemical and biological Engineering, Korea University, Seoul 136-713, South Korea
[c] DTU-Nanotech, Department of Micro and Nanotechnology, Technical University of Denmark, DK-2800 Kongens Lyngby, Denmark

ARTICLE INFO

Article history:
Received 18 November 2011
Accepted 25 November 2011
Available online 6 December 2011

Keywords:
Gold nanoparticles
BRCA-1
Single-mismatched detection
Salt-induced
DNA hybridization

ABSTRACT

In this study, a gold nanoparticle (Au-NP)-based detection method for sensitive and specific DNA-based diagnostic applications is described. A sandwich format consisting of Au-NPs/DNA/PMP (Streptavidin-coated MagnetSphere Para-Magnetic Particles) was fabricated. PMPs captured and separated target DNA while Au-NPs modified with oligonucleotide detection sequences played a role in recognition and signal production. Due to the much lower stability of mismatched DNA strands caused by unstable duplex structures in solutions of relatively low salt concentration, hybridization efficiency in the presence of different buffers was well investigated, and thus, the optimized salt concentration allowed for discrimination of single-mismatched DNA (MMT) from perfectly matched DNA (PMT). Therefore, quantitative information concerning the target analyte was translated into a colorimetric signal, which could easily and quantitatively measured by low-cost UV–vis spectrophotometric analysis. The results indicated this to be a very simple and economic strategy for detection of single-mismatched DNA strands.

1. Introduction

The development of simple and efficient platforms for the rapid detection of nucleic acids for the early diagnosis of various genetic diseases has recently taken precedence (Hacia et al., 1996; Drummond et al., 2003; Cha et al., 2009). Sequence recognition is probably the least understood step in the entire process; small variations in the genome influence biological predisposition to diseases, such as cancer and congenital genetic diseases. Identification of these variations has become a major issue in genetics because they are believed to be major determinants of disease onset, progression, and clinical prognosis (Elghanian et al., 1997; Cui et al., 2001; Park et al., 2009).

Recently, gold nanoparticles (AuNPs) have come under scrutiny as they offer attractive properties as DNA tags (Han et al., 2006; Katz and Willner, 2004; Zhang et al., 2007). AuNPs labeled with oligonucleotide probes to overcome the problems associated with fluorescent labels have shown their important roles in the developments of multiplexing assays and sensors for genetic analyses (Niemeyer, 2001; Rosi and Mirkin, 2005; Bruchez et al., 1998; Han et al., 2001). Further extensive applications in a variety of electronic and optical biosensing systems have much benefited from sensitivity, long lifetime, and multiplexing capability of AuNPs-based assays (Park et al., 2002; Daniel and Astruc, 2004; Boisselier and Astruc, 2009). Mirkin and co-workers have reported several optical DNA hybridization detection methods (Nam et al., 2004; Rosi and Mirkin, 2005), in which most of their research focused on the hybridization-induced DNA-Au aggregates based on the unique size-dependent scattering, catalytic, and absorption properties of AuNPs. This was attributable to their discovery that Au particles, heavily functionalized with oligonucleotides, exhibit extraordinarily sharp thermal-denaturation profiles (Jin et al., 2003). Based on this observation, they developed a thermal-stringency wash approach to differentiate target strands from those bearing mismatches and thus achieved the desired analyte selectivity (Elghanian et al., 1997; Cao et al., 2002). In addition, Mirkin et al. systematically investigated some of the potential factors affecting the melting properties of these novel materials, and a subsequent thermodynamic model was presented to account for the experimental observations (Storhoff et al., 2000). The sharp melting may result from two key factors (Elghanian et al., 1997): the presence of multiple DNA linkers between each pair of nanoparticles; a decrease in the melting temperature as the duplex DNA strands melt due to a concomitant reduction in the local dielectric. The interactions (Alexei and Sergey, 1998) between the neighboring DNA molecules play an important role in DNA hybridization at the interface because the double-helix structure of DNA is surrounded by negative ions in solution that provide a repelling force between the strands. Therefore, the stability of the duplex DNA structure is very sensitive to the surrounding hybridization buffer

* Corresponding author. Tel.: +82 31 3290 4853; fax: +82 2 926 6102.
E-mail address: simsj@korea.ac.kr (S.J. Sim).

0956-5663/$ – see front matter © 2011 Elsevier B.V. All rights reserved.
doi:10.1016/j.bios.2011.11.045

Table 1
Sequences of the oligomers used in this work.

Name	Sequence
Capture probe	5′-GAAACCCTATGTATGCTCTTTTTTTTT-Biotin-3′
Detection probe	5′-Amino-(C6)-TTTTTTTTTTTTTTTGTATGAATTATAATCAAA-3′
Target DNA	5′-GAGCATACATAGGGTTTCTCTTGGTTTCTTTGATTATAATTCATAC-3′
Single-mismatched DNA	5′-GAGCATACATAGGGTTTCTCTTGGTTTCTTTGATTATXATTCATAC-3′ (“X” stands for T, C, G)
Non-cognate DNA	5′-ACACGCTTGGTAGACTTTTTTTTTTAGCATCGATAACGTT-3′

The sequence of the target DNA is a segment from the wild-type BRCA-1 gene.

(Yang et al., 2006). And at the solid–liquid interface, many factors such as surface strand density, surface charge, point mismatch, and DNA length result in interfacial heterogeneity and can influence the kinetics and stability of DNA hybridization. These factors make the hybridization and dissociation kinetics of the DNA at the interface much more complicated than free DNA in solution (Jin et al., 2003).

The stability of Au-NPs was investigated in various concentrated salt solutions. Herein, we report a new nanoparticle-based assay for discriminating single-mismatched DNA in a homogeneous solution based on the salt-induced DNA hybridization detection of Au-NPs tags. In this study, because the specificity and sensitivity of this assay were dependent on the stability of the duplex DNA structure after hybridization in different surrounding media (Milam et al., 2003; Rogers et al., 2005), the hybridization processes of random-coil oligonucleotides were studied systematically to evaluate the relative importance of the salt concentration that contributes to hybridization efficiency. In addition to the observed sharp hybridizing transitions, the assay relied on the absorbance signals of unhybridized nanoprobes left over from the oligonucleotide-functionalized gold nanoprobes that directed recognition of the target DNA. This derived, sharp curve for the DNA and Au-NP system proved vital for allowing this method to discriminate single-mismatched DNA targets from the complementary sequence by adjusting salt concentration of the hybridization buffer. The use of salt concentration as a stringency tool may eliminate the need for thermocyclers in gold-based detection systems and presents opportunities for using probes that suffer from instability at elevated temperatures. To examine the assay, breast cancer type 1 gene (BRCA-1) was chosen as the typical target analyte, given its valuable signature in the diagnosis of breast cancer (Gaiser et al., 2004; Rodriguez et al., 2007). We hope such a sandwich design would offer a simple, sensitive, and commercial method for rapid and direct single-mismatched DNA detection in the solution phase, and could potentially contribute to the development of the next generation of DNA diagnostic tools for early stage detection of genetic diseases.

2. Experimental

2.1. Chemicals and materials

Hydrogen tetrachloroaurate trihydrate ($HAuCl_4{\cdot}3H_2O$, 99.9%), sodium citrate, *N*-hydroxysuccinimide (NHS), 1-ethyl-3-(3-dimethylaminopropyl)carbodiimide (EDC), bovine serum albumin (BSA), polyethylene glycol (PEG, Avg. MW 2000), and phosphate buffer saline pH 7.4 (0.01 M PBS buffer solution) were obtained from Sigma–Aldrich (Korea). The $HS(CH_2)_{11}(OCH_2CH_2)_6OCH_2COOH$ (EG_6—COOH) and $HS(CH_2)_{11}(OCH_2CH_2)_3OH$ (EG_3—OH) were purchased from Cos Biotech (Korea). Streptavidin-coated MagnetSphere Para-Magnetic Particles (PMPs) (ca., 1.0 μm diameter, 1.0 mg/mL) were purchased from Promega Corporation (Madison, WI, USA) and hybridization buffer (0.5 M NaCl, 4% blocking reagent) from Biosesang, Inc. (Korea). When required, all chemical solutions and buffers were prepared in ultra-pure water (18.2 mΩ/cm). All synthetic oligonucleotides were purchased from Genotech Corporation (Korea) as shown in Table 1.

Optical absorbance intensity was measured using a life science UV–vis scanning spectrophotometer (DU730, Beckman Coulter, Inc., USA). A hybridization incubator (combi-H12) and a Twist shaker (TW13) were purchased from Finemould precision Ind. Co. (Seoul, Korea). The size of the Au-NPs was measured by transmission electron microscopy (JEM3010). The multipurpose refrigerated centrifuge (VS-5500CFN, 15CFN) was from Vision Scientific Co. Ltd. (Seoul, Korea).

2.2. Preparation of the gold colloid

The Au-NPs were synthesized by reducing $HAuCl_4$ with sodium citrate according to previous methods (Grabar et al., 1995), with slight modifications. Briefly, under vigorous stirring, 20 mL of the 0.25 mM $HAuCl_4$ solution was heated until boiling. Rapid addition of 2.0 mL of 5.0 mM sodium citrate solution resulted in a continuous color change from colorless to red; stirring was continued for the next 10 min after the color change ceased; the heating source was then removed and the stirring continued for another 15 min. The evaporated water was compensated with DI water once the solution cooled down to room temperature. The final solution was filtered through a 0.2 μm membrane filter and stored at 4 °C.

2.3. Preparation of OEG-stabilized gold nanoprobes

A previous procedure for the formation of oligo(ethylene glycol)-terminated SAMs on a bare gold surface (Cao et al., 2006; Cao and Sim, 2007a, b) was employed in this work with slight modifications. The Au-NPs were first modified with a mixture of EG_6—COOH and EG_3—OH by our group (Zhan et al., 2010) according to the following procedure: 1.0 mL absolute ethanol solution containing a 1:9 molar ratio of EG_6—COOH/EG_3—OH was added to 9.0 mL of Au-NPs solution to a final concentration of 0.5 mM. A mixed SAM on the gold surface was formed after overnight incubation with gentle shaking at room temperature. Next, the mixture was centrifuged (14,000 rpm, 30 min, 4 °C), the supernatant was decanted, and the pellet was rinsed with PBS (0.01 M, pH 6.0). This centrifugation/resuspension step was repeated >3 times to remove the ethanol and unbound OEG molecules, and the final carboxyl-stabilized Au-NPs solution was concentrated to 5.0 mL. Subsequently, 100 μL of 0.1 M NHS was immediately added after being activated with 100 μL of a 0.1 M EDC solution and incubated for 10 min. Afterwards, the amine-functionalized DNA detection probe was added to the solution to a final concentration of 0.5 μM. The mixed solution was again incubated for 8 h at room temperature with gentle shaking, and the centrifugation/rinsing procedure was repeated 3 times to remove unbound DNA probe. The final pellet was suspended in 5.0 mL of PBS buffer solution (0.01 M, pH 7.4) and stored at 4 °C until further use.

2.4. Preparation of PMP capture probes

Para-streptavidin-modified magnetic micro-particles were first washed 2 times with washing buffer and then conjugated with the biotinylated capture DNA using the protocol provided by the manufacturer. The mixture (at a ratio of 1.0 nmol probe to 0.6 mL

PMPs) was incubated for 30 min at room temperature with gentle shaking and washed 2 times with 0.5 mL blocking solution (0.01 M PBS solution contained 2% BSA and 5% PEG) to block nonspecific binding. The mixture was washed again after 30 min of incubation and finally stored in a 0.5 mL stock solution (0.01 M PBS solution contained 1% BSA) at 4 °C until further use.

2.5. DNA hybridization procedure

In a typical experiment, 50 μL of capture probe-coated PMPs were added into a 1.5 mL micro-centrifuge tube and magnetically collected after washing with hybridization buffer. Then, 100 μL of the DNA solutions were added and incubated with the PMPs for 1 h at 37 °C with gentle shaking. Then, the collection and washing steps were repeated 3 times to thoroughly remove the unhybridized DNA strands. Subsequently, 100 μL of the Au nanoprobe detecting solution (50 μL hybridization buffer, 50 μL nanoprobes) was added to the tube and the mixture was incubated for another 1 h to ensure all target segments were recognized. The complexes were then magnetically separated and carefully washed 3 times with 200 μL of washing buffer to remove the excessive Au nanoprobes. Notably, these buffer solutions, as well as the unhybridized nanoprobes, were collected into a new cuvette to measure the absorption signals.

2.6. Determination of salt concentration on hybridization efficiency

Effects of salt concentration were investigated by adding a series of different concentrations of salt solution as a hybridization buffer in the detection step. Briefly, 50 μL of nanoprobes were incubated with 50 μL of various Na^+ concentrations of PBS solutions, ranging from 0.2 to 1.0 M, in an Eppendorf tube. Thus, the final concentration of the hybridization buffer was diluted to half (0.1–0.5 M). The reaction continued for 1 h at 37 °C with gentle mixing. Finally, following three washes, the upper aqueous solution containing the unhybridized nanoprobes was obtained and transferred to a 1.0 mL cuvette.

2.7. Experimental procedures for BRCA-1 detection

Fig. 1 describes the experimental strategies used in this study where the target DNA was first captured by direct hybridization with biotin-labeled DNA magnetic particles (step 1). Following separation of the captured target DNA, the Au-NP labeled nanoprobes were added for target identification (step 2). Consequently, using a permanent bar magnet, the DNA-linked particles (hybridized complex) were separated (step 3) and the unhybridized nanoprobes were collected and transferred to a cuvette for spectroscopic measurement (step 4). It is important to note that sufficient and careful washing is extremely crucial throughout the entire experiment. Subsequently, the final signals of absorbance intensity, which depend on the amount of unhybridized gold nanoprobes, were easily recorded with a UV–vis spectrophotometer.

3. Results and discussion

3.1. Characterization of gold nanoprobes

The UV–vis spectra of the Au-NPs are shown in Fig. 2. The absorption peak at 521 nm was assigned to 15 nm unmodified spherical gold nanoparticles, attributed to the typical plasmon band of the nanoscale gold. Comparison of the initial gold salt concentration to the average particle diameter obtained from TEM measurements yielded the final Au-NPs solution concentration, which was ~4.0 nM (Cao et al., 2011). After surface modification of Au-NPs,

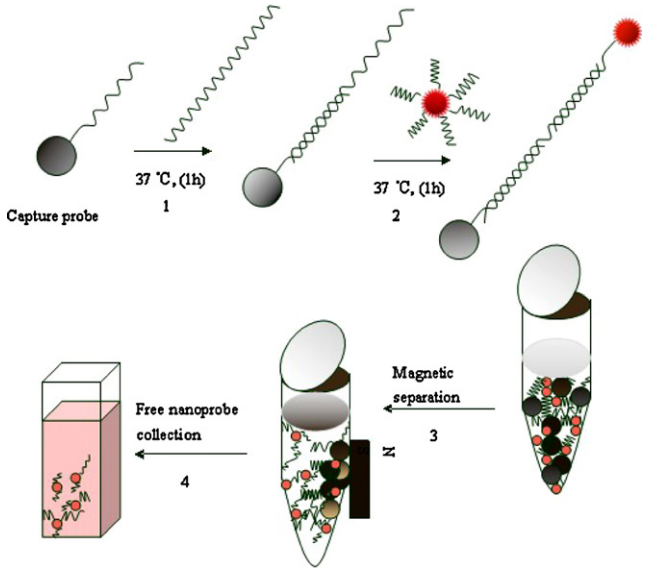

Fig. 1. Schematic illustration for the entire experimental strategy for BRCA-1 detection.

only a slight shift in the surface plasmon band from 521 to 525 nm was observed. The plasmon band of a complex detection probe (Au-OEG-DNA) centered at 527 nm also indicated a small red shift. It is a fact that the position of the plasmon band is very sensitive to the size and surrounding environment of the Au-NPs (Bianmei et al., 2011). However, in this experiment, only small changes in the surface plasmon bands were obtained after the conjugations, thus confirming the simple and timesaving conjugation method that was offered as a promising and effective surface modification of the Au-NPs for ultrasensitive DNA detection.

It is known that when prepared by reduction of $HAuCl_4$ using sodium citrate as a reducing agent, gold colloid nanoparticles are surrounded by a negative-charge layer arising from the residual negative citrate ions in solution. This charge layer can be

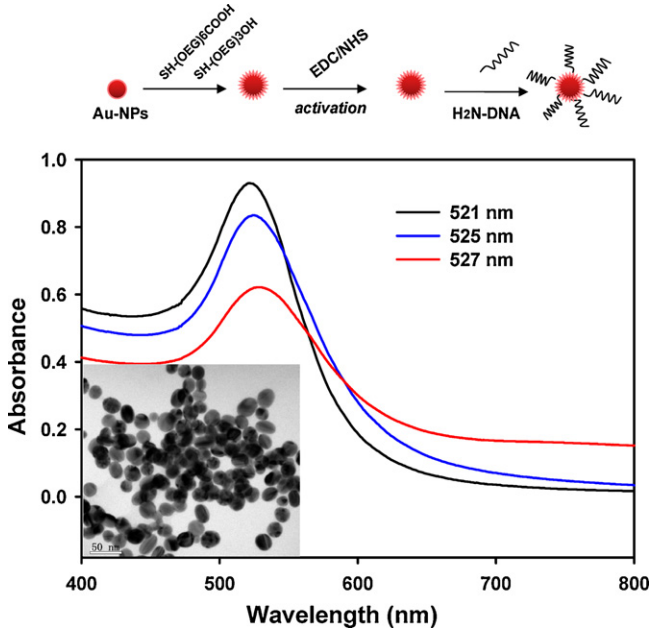

Fig. 2. Scheme of the nanoprobe preparation and comparison of UV–vis spectra for colloidal gold nanoparticles in aqueous solution, OEG-functionalized AuNPs, and nanoprobes in PBS solution. The inset image shows the size of colloidal gold nanoparticles.

compressed or expanded depending on the total ionic concentration of the surrounding solution (Zhang et al., 2008). The unmodified gold nanoparticle colloid is unstable upon exposure to high concentrations of electrolyte because highly concentrated electrolytes compress the charge layer. For example, when added into a 0.5 M NaCl solution, an aqueous solution of unmodified gold nanoparticles quickly turns from red to blue, indicating aggregation. Therefore, the quality of the self-assembly monolayer is crucial for the nanoprobes because it not only maintains particle stability, but also protects the surface from nonspecific adsorption. However, previous studies have shown that steric crowding on densely DNA oligomer-modified surfaces can limit hybridization efficiency, because electrostatic repulsions and steric hindrance cause low accessibility for the probes to enter hybridizing strands on the highly loaded Au-NPs (Demers et al., 2000). To our experience, it is vital to note that the strategy used here, which simultaneously provides a functionalized group and a spacer, could greatly improve hybridization efficiency by precisely controlling the surface monolayer via the OEG mixture. Because the assembly of ss-DNA requires high concentrations of NaCl, but the unmodified gold nanoparticles are unstable under such conditions. Thus, this flexible linker system could not only provide a large number of reactive binding sites to increase sensitivity, but also, the high background intensities caused by nonspecific binding during hybridization were avoided. The greater stability of the surface-oligonucleotide complex in the case of the nanoparticle system presumably results in less target and probe loss during downstream washing steps. This immobilization method may be used for different bioaffinity assays (magnetic collection and detection of immuno-linked particle networks) and to other liquid-phase optical applications.

3.2. Effect of salt concentration

Sodium salt played a dual role in the stability of Au-NPs (Han et al., 2008). This effect is actually similar to the "salt-in" and "salt-out" behavior of protein molecules. At low salt concentration, NaCl prevented the formation of AuNP aggregates, further increases in NaCl concentration also caused the AuNP finally to aggregate as a result of decreased electrostatic repulsion between AuNPs. The continued addition of NaCl to reach a certain concentration could disrupt the already formed AuNP aggregates. In Fig. 3A, the UV–vis spectra of the colloidal gold nanoparticles in various concentrations of salt showed the overall shapes of the spectra were not obviously altered, with the exception of some decrease in the absorbance. This indicated AuNPs were not aggregating under the salt concentration from 0.1 to 0.5 M.

Based on the evaluation of gold nanoprobes in sodium salt solution above, the authors investigated an unusual salt dependence of the hybridization efficiency of the hybridized gold nanoprobe. As shown in Fig. 3B, a key issue in this method pertains to the use of certain hybridization buffers to describe the different efficiencies during the hybridization process. Notably, hybridization of 2 single-stranded DNA (ssDNA) molecules into a duplex of double-stranded DNA (dsDNA) and its dissociation back into 2 single strands are essential to many DNA-related technologies. Two DNA fragments with homologous sequences can form a favorable alignment with negatively charged strands facing positively charged grooves. This creates surface charge separation with excess negative charge on the phosphate strands and an excess of positive charge in the grooves. Note that even mobile counterions, such as Na^+, tend to condense in DNA grooves because of the combination of hardcore and electrostatic interactions (Kornyshev and Leikin, 2001). The rate-limiting step of oligonucleotide hybridization is the formation of a few base pairs from each strand into a transient intermediate called a nucleus. The remaining bases will then quickly form a complete helix. Therefore, to determine the

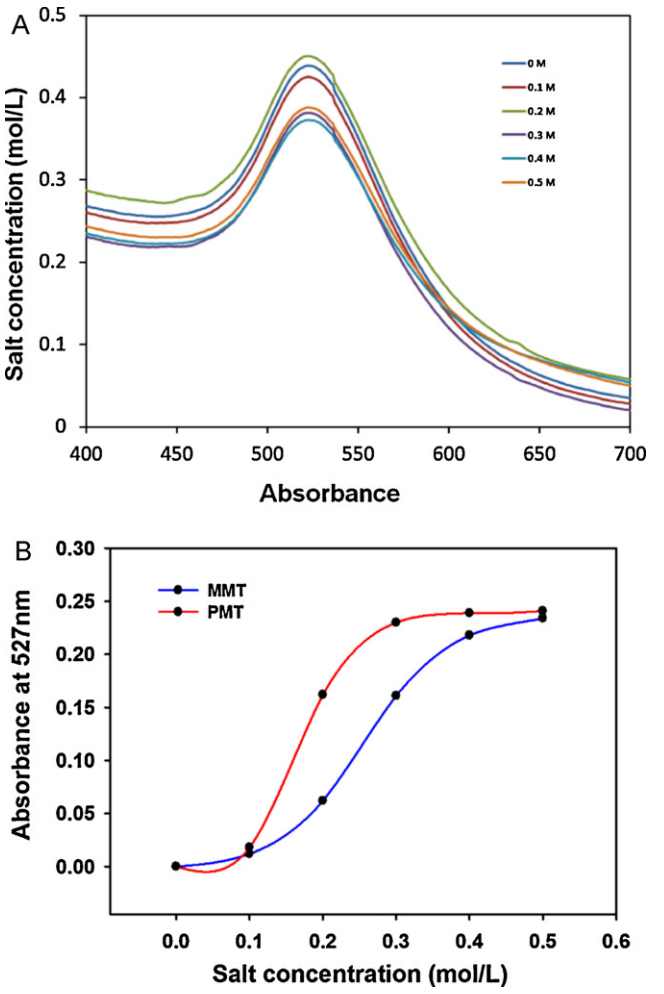

Fig. 3. (A) Absorbance spectra of gold nanoprobe in various concentrations of salt. (B) Effect of salt concentration on DNA hybridization efficiency. (Experimental condition: nanoprobes 50 μL; Na^+ concentrations of HB range from 0.1 to 0.5 M; hybridization 1 h at 37 °C.)

effect of increasing salt concentration on the hybridization efficiency of a DNA-linked nanoparticle system, the kinetic behavior of hybridization was studied as a function of Na^+ concentration. As the salt concentration increased from 0.1 to 0.5 M, while keeping the nanoparticle and target concentrations constant, the deduced optical absorbance subsequently increased. This is consistent with the conclusion that the increased dielectric created by the higher salt concentration hybridization buffer stabilizes the duplex DNA interconnections. This is likely due to the highly ionic effect of the salt, which is attributed to the stability of the DNA duplex structure, allowing more hybridization events to occur. Another reason is the screening effect of the salt, which minimizes electrostatic repulsion between the oligonucleotide-modified particles, also leading to more hybridization events between the targets and nanoprobes and hence, greater accumulation of the surface plasmon absorption of the Au-NPs. This screening effect was also reflected in an experiment designed to study the hybridization rates as a function of salt concentration. Fig. 3B shows 2 sets of particles functionalized with capture probes and detection probes, respectively (Table 1). The target DNA was dispersed in PBS buffer (10 mM phosphate, pH 7) at salt concentrations of 0.1, 0.2, 0.3, 0.4, and 0.5 M, respectively. The hybridization rate was studied by monitoring the absorbance intensity of the surface plasmon resonance at 527 nm for 15 nm gold nanoprobes as a function of Na^+ concentration. As indicated in Fig. 3B, the hybridization rate

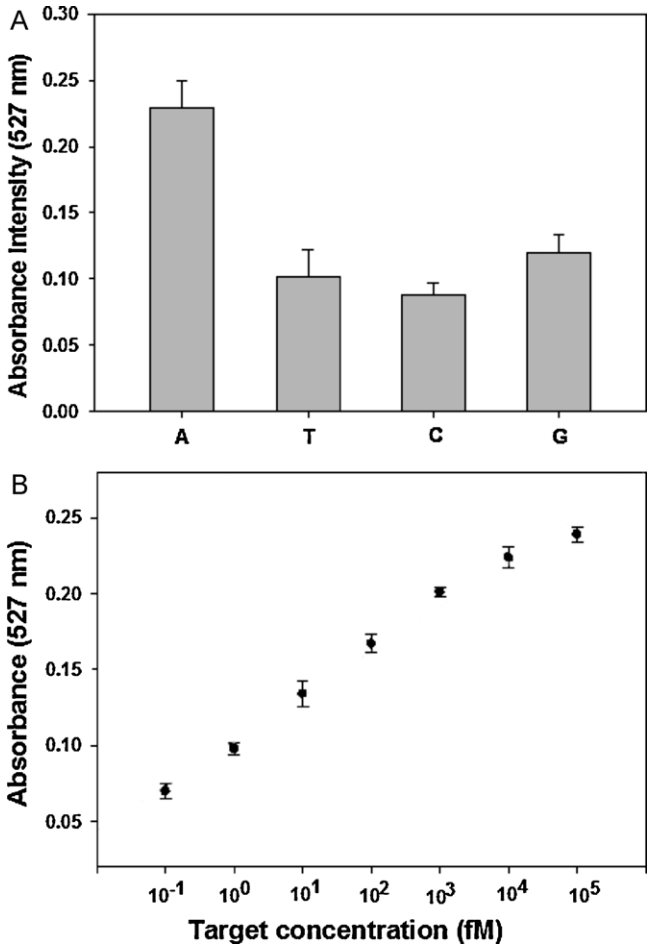

Fig. 4. (A) Nanoprobe-based colorimetric detection for single-base mismatches. (Experimental condition: target DNA 10 pM; Na^+ concentrations of HB 0.25 M; hybridization 1 h at 37 °C.) (B) Absorbance intensity in colorimetric detection of target DNA spanning a 0.1 fM to 100 pM concentration range. (Experimental condition: target DNA 100 aM to 100 pM; Na^+ concentrations of HB 0.25 M; hybridization 1 h at 37 °C.)

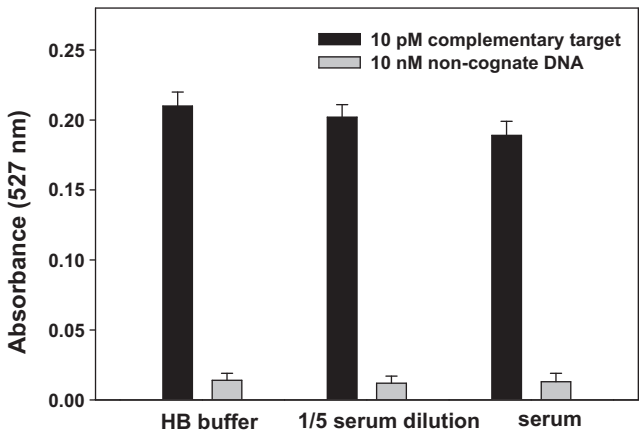

Fig. 5. Detection of 10 pM DNA target (black bars) and 10 nM non-cognate DNA (gray bars) in buffer, 1/5 diluted serum, and undiluted serum. (Experimental condition: target DNA 10 pM; Non-cognate DNA 10 nM; Na^+ concentrations of HB 0.25 M; hybridization 1 h at 37 °C.)

was markedly dependent on and directly proportional to increasing salt concentration. These data clearly demonstrate that the electrostatic interactions between the nanoparticles, which can be tailored by adjusting the salt concentration, play an important role in their hybridization behaviors. These observations enable control over the DNA-nanoparticle hybridization/dehybridization processes by adjusting salt concentration at or above room temperature. The salinity of the hybridization buffer can be selected so that a high proportion of labeled probe can hybridize to perfectly matched target DNA strands, while most of the mismatched strands could not be easily hybridized to nanoprobes. As shown in Fig. 3B, the signal changed dramatically and the difference in the hybridization efficiency increased over time. A maximum difference appeared at 0.25 M, and the absorbance intensity could not further increase beyond a buffer concentration of 0.4 M. This relationship is well defined thus it is possible to control the maximum extent of hybridization of the nanoparticle probes. Therefore, a concentration of 0.25 M Na^+ PBS buffer solution for the hybridization process was chosen for the remaining experiments described herein.

3.3. Discrimination of single mismatches

As mentioned earlier, controlling the ionic strength would be expected to differentiate the single-base mutation from perfectly complementary targets. Oligonucleotide-modified nanoparticles usually exhibit sharp hybridization properties over salt concentration gradients. Significantly, the hybridization mainly occurs over a narrow salt concentration (0.1 M) range and can be used to readily discriminate between perfectly complementary targets and single-base mismatched strands. And thus, 4 different single-mismatched bases of target DNA were designed to detect under the same conditions (0.25 M Na^+). As the results showed in Fig. 4A, the different target DNA and nanoprobes successively hybridized to the capture probes in the hybridization buffer. It is noteworthy that the detection nanoprobes hybridized to the different target elements in the order of the predicted stability of the Watson–Crick base pairs: A:T complement first, followed by the G:T wobble pair, and finally by the C:T and T:T mismatches (Park et al., 2002; Zhang et al., 2007). The relative ratios of nanoprobes hybridized to different elements of the targets determined the overall effectiveness of the method for discriminating between different target sequences. In principle, the greater the difference in binding affinity at a given temperature between a complex containing a perfect target and one with a mismatched base, the higher this ratio and the better the discrimination. These unusually narrow salt-induced hybridization transitions involving nanoparticles are important because they can be used to develop high selectivity detection assays and potentially eliminate the need for thermal stringency. The authors found that oligonucleotide-functionalized nanoparticles exhibit unique hybridization properties that can lead to improved selectivity of the DNA biosensor.

3.4. Hybridization signal intensity versus DNA concentration

The quantitative behavior was assessed by monitoring the dependence of the nanoprobe hybridization signal vs. concentration of the target oligonucleotide. As shown in Fig. 4B, well-defined signals, proportional to the target concentration, were observed over a range of 100 aM to 100 pM (after 1 h hybridization). The linearity determined from 100 aM to 100 fM is much better than that from 1 pM to 100 pM because absorbance values measured in that range are already saturated. Such a sensitive detection method reflects the amplification features of gold nanoparticle tags and compares favorably to values reported for other particle-based DNA assays (Nam et al., 2004; Zhang et al., 2007). To investigate the selectivity of the presented assay system, the immunosensor was incubated in the incubation solution containing different concentrations of target and various concentrations of non-cognant DNA. The results show that non-cognant DNA below some tolerance

limit in normal human serum samples does not appreciably interfere with sensor response (Fig. 5). A series of 5 repetitive measurements of the 10 pM breast cancer gene target solution, used for estimating precision, yielded reproducible signals with a relative standard deviation of 7%. Thus, the sensor had a good selectivity to BRCA-1, as well as acceptable regeneration efficiency. With respect to the signal intensities obtained from the hybridization experiment, these findings may be applied towards determination of BRCA-1 in human serum for routine clinical diagnosis.

4. Conclusions

In summary, we have demonstrated a new gold nanoparticle-based strategy for detecting sequence-specific DNA in a homogeneous solution. This method was dependent on the stability of the duplex DNA structure in different surrounding media and therefore the effects of the salt concentration in the hybridization buffer on DNA hybridization were thoroughly investigated. As an optimum stringency was approached with the nanoprobes, most of the capture-target complex was hybridized with detection probes, leaving little signal to monitor. The derived, sharp hybridization curve was obtained since the absolute signal intensity at the complementary (A) element was greater for the nanoparticle array at salt concentrations of optimum stringency. With the proposed salt-induced hybridization assay, the single-base mismatched DNA strands of BRCA-1 could be directly discriminated from the perfectly complementary targets without stringent control over temperature. As expected, such a simple, sensitive, and commercial method could be potentially applied to predict the risk of early breast cancer by identifying single mismatched DNA strands of BRCA-1.

Acknowledgements

This work was supported by the Korea Science and Engineering Foundation (KOSEF), National Research Laboratory (NRL) Program (R0A-2008-000-20078-0), Basic Science Research Program (2010-0027771) and a grant (DG2-201) from the Carbon Dioxide Reduction & Sequestration Research Center, one of the 21st Century Frontier Programs funded by the Ministry of Science and Technology of the Republic of Korea.

References

Alexei, A.K., Sergey, L., 1998. Proc. Natl. Acad. Sci. U.S.A. 95, 13579–13584.
Bianmei, C., Tingfei, X., David, H., 2011. AMES 17 (2), 79–85.
Boisselier, E., Astruc, D., 2009. Chem. Soc. Rev. 38, 1759–1782.
Bruchez, M., Moronne, M., Gin, P., Weiss, S., Alivisatos, A.P., 1998. Science 281, 2013–2016.
Cao, C., Gontard, L.C., Tram, L.L.T., Wolff, A., Bang, D.D., 2011. Small 7, 1701–1708.
Cao, C., Kim, J.P., Kim, B.W., Chae, H.Y., Yoon, H.C., Yang, S.S., Sim, S.J., 2006. Biosens. Bioelectron. 21, 2106–2113.
Cao, C., Sim, S.J., 2007a. Biosens. Bioelectron. 22, 1874–1880.
Cao, C., Sim, S.J., 2007b. J. Nanosci. Nanotechnol. 7, 3754–3757.
Cao, Y.W.C., Jin, R., Mirkin, C.A., 2002. Science 297, 1536–1540.
Cha, B.H., Lee, S.M., Park, J.C., Hwang, K.S., Kim, S.K., Lee, Y.S., Ju, B.K., Kim, T.S., 2009. Biosens. Bioelectron. 25, 130–135.
Cui, Y., Wei, Q., Park, H., Lieber, C.M., 2001. Science 293, 1289–1292.
Daniel, M.C., Astruc, D., 2004. Chem. Rev. 104, 293–346.
Demers, L.M., Mirkin, C.A., Mucic, R.C., Reynolds, R.A., Letsinger, R.L., Elghanian, R., Viswanadham, G., 2000. Anal. Chem. 72, 5535–5541.
Drummond, T.G., Hilland, M.G., Barton, J.K., 2003. Nat. Biotechnol. 21, 1192–1199.
Elghanian, R., Storhoff, J.J., Mucic, R.C., Letsinger, R.L., Mirkin, C.A., 1997. Science 277, 1078–1080.
Gaiser, O.J., Ball, L.J., Schmieder, P., Leitner, D., Strauss, H., Wahl, M., Kühne, R., Oschkinat, H., Heinemann, U., 2004. Biochemistry 43, 15983–15995.
Grabar, K.C., Freeman, R.G., Hommer, M.B., Natan, M.J., 1995. Anal. Chem. 67, 735–743.
Hacia, J.G., Brody, L.C., Fodor, S.P.A., Collins, F.S., 1996. Nat. Genet. 14, 441–447.
Han, M.S., Lytton-Jean, A.K.R., Mirkin, C.A., 2006. Angew. Chem. Int. Ed. 45, 1807–1810.
Han, M.Y., Gao, X.H., Su, J.Z., Nie, S., 2001. Nat. Biotechnol. 19, 631–635.
Han, X., Li, Y., Wu, S., Deng, Z., 2008. Small 4, 326–329.
Jin, R., Wu, G., Li, Z., Mirkin, C.A., Schatz, G.C., 2003. J. Am. Chem. Soc. 125, 1643–1654.
Katz, E., Willner, I., 2004. Angew. Chem. Int. Ed. 43, 6042–6108.
Kornyshev, A.A., Leikin, S., 2001. Phys. Rev. Lett. 86, 3666–3669.
Milam, V.T., Hiddessen, A.L., Crocker, J.C., Graves, D.J., Hammer, D.A., 2003. Langmuir 19, 10317–10323.
Nam, J.M., Stoeva, S.I., Mirkin, C.A., 2004. J. Am. Chem. Soc. 126, 5932–5933.
Niemeyer, C.M., 2001. Angew. Chem. Int. Ed. 40, 4128–4158.
Park, J.S., Cho, M.K., Lee, E.J., Ahn, K.Y., Lee, K.E., Jung, J.H., Cho, Y.J., Han, S.S., Kim, Y.K., Lee, J., 2009. Nat. Nanotechnol. 4, 259–264.
Park, S.J., Taton, T.A., Mirkin, C.A., 2002. Science 295, 1503–1506.
Rodriguez, H., Jaruga, P., Leber, D., Nyaga, S.G., Evans, M.K., Dizdaroglu, M., 2007. Biochemistry 46, 2488–2496.
Rogers, P.H., Michel, E., Bauer, C.A., Vanderet, S., Hansen, D., Roberts, B.K., Calvez, A., Crews, J.B., Lau, K.O., Wood, A., Pine, D.J., Schwartz, P.V., 2005. Langmuir 21, 5562–5569.
Rosi, N.L., Mirkin, C.A., 2005. Chem. Rev. 105, 1547–1562.
Storhoff, J.J., Lazarides, A.A., Mucic, R.C., Mirkin, C.A., Letsinger, R.L., Schatz, G.C., 2000. J. Am. Chem. Soc. 122, 4640–4650.
Yang, Gao, Wolf, Lauren K., Georgiadis, Rosina M., 2006. Nucleic Acids Res. 34, 3370–3377.
Zhan, Z., Cao, C., Sim, S.J., 2010. Biosens. Bioelectron. 26, 511–516.
Zhang, H.L., Qiao, F.Y., Liu, J., Li, F.R., Kong, X.L., Zhou, H.X., 2008. Appl. Surf. Sci. 254, 2941–2946.
Zhang, J., Song, S.P., Wang, L.H., Pan, D., Fan, C.H., 2007. Nat. Protoc. 2, 2888–2895.